Mitotic Membrane Helps to Focus and Stabilize the Mitotic Spindle

Christopher C. Poirier,[†] Yixian Zheng,[‡§] and Pablo A. Iglesias[†*]
[†]Department of Electrical and Computer Engineering, The Johns Hopkins University, Baltimore, Maryland; and [‡]Department of Embryology, Carnegie Institution of Washington and [§]Howard Hughes Medical Institute, Baltimore, Maryland

ABSTRACT During mitosis, microtubules (MTs), aided by motors and associated proteins, assemble into a mitotic spindle. Recent evidence supports the notion that a membranous spindle matrix aids spindle formation; however, the mechanisms by which the matrix may contribute to spindle assembly are unknown. To search for a mechanism by which the presence of a mitotic membrane might help spindle morphology, we built a computational model that explores the interactions between these components. We show that an elastic membrane around the mitotic apparatus helps to focus MT minus ends and provides a resistive force that acts antagonistically to plus-end-directed MT motors such as Eg5.

INTRODUCTION

The assembly of microtubules (MTs) into the mitotic spindle during mitosis represents one of the most fascinating examples of self-association in cellular biology. It is now understood that mitotic spindle formation is driven by MT-based motors, aided by MT-binding nonmotor proteins, and diffusive gradients. Recent experiments have provided evidence that membranous networks, including the spindle matrix, may also have a role in spindle formation (1–4). The spindle matrix consists of molecules and proteins that do not directly interact with MTs but may play a role in the assembly and organization of the mitotic spindle. How this membranous network may aid spindle formation is less clear.

Despite progress in discovering the players involved in forming the spindle, the mechanism by which MTs interact to form the bipolar structure remains an open question. The complexity of this issue has led researchers to turn to a number of computational models to test some basic hypotheses (5,6). For example, computational models suggested that only in the presence of hybrid motors consisting of both plus- and minus-end-directed motors could antiparallel MT assemblies that roughly resemble the mitotic spindle arise (7). Subsequent simulations suggested that spatial differences in the parameters that dictate MT interactions—for example, those that describe MT dynamic instability or motor diffusion within the spindle—increase the amount of antiparallel MT interaction and lead to spindles with improved morphology (8). The identity of these hybrid motors, however, remains unknown. More recently, a theoretical and experimental study showed that the lamin-based mitotic matrix may help to stabilize the mitotic spindle by providing a balance to the force generated by the MT-associated motors (9).

We developed a multiagent simulation environment that includes MTs, discrete plus- and minus-end-directed motors, and a viscoelastic enclosing membrane to characterize the roles that a membrane might play in formation of the mitotic spindle. Here we use this model to show that, in addition to providing a scaffold that pushes against MTs to aid in force balancing, the presence of an elastic membrane surrounding the MTs helps to focus them into a spindle.

MATERIALS AND METHODS

We developed an agent-based computational model that tracks discrete interactions between flexible astral and free MTs, plus-end- and minus-end-directed motors, and a viscoelastic membrane (Fig. 1 *A*, Table 1). The MTs are subject to a range of forces, including those from molecular motors, interactions through collision with the enclosing membrane, and thermal fluctuations. Each MT is inextensible but subject to lateral fluctuations in two dimensions based on its flexural rigidity. The motors diffuse when unbound, bind and unbind to the MTs and the membrane (minus-end motors only), or move along the MTs. The passive membrane generates force when deformed from its initial circular shape.

All molecular species are contained within a 32×32 μm bounding box. Periodic boundary conditions were used to track motors that diffused through the boundaries. Simulations were carried out for 20 min in time steps of 100 ms. Simulations were conducted with the use of MATLAB (The MathWorks, Natick, MA) on Intel Xeon Quad Core Processors with 8GB of RAM. The total simulation time per calculation run was ~6 h.

Microtubules

We include two types of MTs. Astral MTs are attached at their minus ends and initially radiate outward with a direction based on a sampling of a uniform distribution. The length of each astral MT is also chosen randomly from a uniform distribution between 2 and 5 μm. Two asters are initially positioned randomly, subject to the constraints that they must be at opposite sides of the cell and all astral MTs must be contained wholly within the membrane. Additionally, a number of free MTs of fixed length are placed randomly with the constraint that there must be an equal number of minus ends in each half of the cell, with each filament having a random orientation while still being contained with the cell boundary.

To model each MT, an integer number of fixed-length (250 nm) inelastic segments are used. Because not all filaments are of the same length, each filament, j, contains M_j segments and is described by the $M_j + 1$ nodes connecting the segments. The MTs move and bend subject to external forces and thermal motion as previously described (7,8,10).

Submitted June 22, 2010, and accepted for publication September 27, 2010.

*Correspondence: pi@jhu.edu

Editor: Leslie M. Loew.

0006-3495/10/11/3182/9 $2.00

doi: 10.1016/j.bpj.2010.09.053

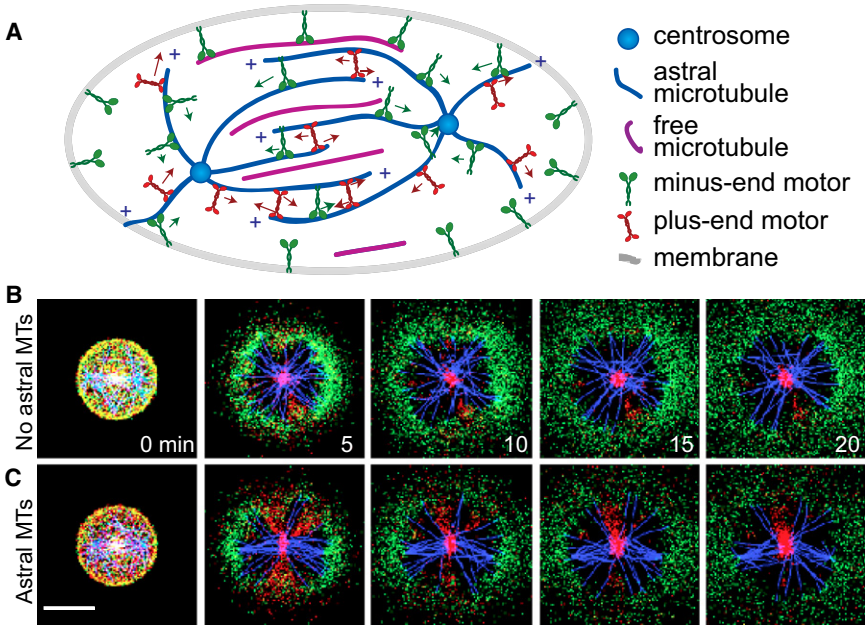

FIGURE 1 Mitotic spindle apparatus inside a closed membrane. (*A*) Schematic of the components included in the model. In the simulations that follow, the MTs (both astral and free) are shown as rods and the plus- and minus-end-directed motors are shown as dots. (*B* and *C*) Sample simulations of a cell, where the mitotic spindle apparatus is not enclosed by a shell for cells both without (*B*) and with (*C*) centrosomes. In both cases the minus-end motors are pushed to the periphery, where they fall off the MT minus ends. Thereafter, they diffuse away from the center of the cell. The plus-end motors congregate toward the center. The MTs do not organize into spindles. The scale bar represents 5 μm.

Membrane

The mitotic membrane is represented by an impenetrable, deformable barrier enclosing the motors and MTs. Initially a circle 8 μm in diameter, it has both viscous and elastic properties. Its strain characteristics are based on in vitro measurements of the nuclear envelope strain (11) with elastic modulus k_{mem} and an assumed viscosity η_{mem} (10-fold higher than that of the cytoplasm, η_{cyto}).

TABLE 1 Default simulation parameters

Symbol	Parameter	Value	Units	Reference
N_{MT}	Number of MTs	50		(8)
N_{aster}	Number of astral MTs (per aster)	15		
N_{free}	Number of free MTs	20		(32)
l_{fill}	Length of free MTs	5	μm	(32)
R_{mem}	Initial radius of the membrane	4	μm	
k_{mem}	Elastic modulus of membrane	200–390	pN/μm	(11)
η_{cyto}	Viscosity of cytoplasm	50×10^{-3}	pN μm^2	(8)
η_{mem}	Viscosity of membrane	$10\eta_{cyto}$	pN μm^2	estimate
r_{grid}	Grid resolution	187.5	nm	
r_{motor}	Motor capture radius	10	nm	(32)
D_{motor}	Motor diffusion coefficient	0.04	μm^2/s	(8,13)
F_{DynNL}	No-load minus-end motor force	0	pN	
F_{DynL}	Loaded minus-end motor force	4	pN	(33)
v_{DynNL}	No-load minus-end motor velocity	0.8	μm/s	(33,34)
v_{DynL}	Loaded minus-end motor velocity	0.2	μm/s	(33)
F_{KinNL}	No-load plus-end motor force	0	pN	
F_{KinL}	Loaded plus-end motor force	2	pN	(13)
v_{KinNL}	No-load plus-end motor velocity	0.08	μm/s	(13)
v_{KinL}	Loaded plus-end motor velocity	0.02	μm/s	(13)
k_{con}	Elastic modulus of motor connections	20	pN/ μm	
r_c	Interaction radius of membrane	50	nm	
Δt	Time step	100	ms	(7,8)

The membrane and MTs interact through membrane-tethered minus-end motors and MT/membrane collisions. The membrane can bend, having a flexural rigidity on the same order of MTs. To compute the membrane interactions, the membrane is divided into 200 discrete segments, each initially ~125 nm in length. Each segment is defined by two nodes, with the combination of all such nodes forming a circular chain. Forces acting on the membrane are distributed to the closest nodes weighted proportionally by the respective proximities. Membrane bending is computed via the position of successive triplets of points, with rounding force proportional to the computed bending moment. The total force on the nodes and the viscoelastic properties are used to determine the resulting membrane deformation.

Motor interactions

We consider two types of motors: plus-end-directed motors (e.g., Eg5) and minus-end-directed motors (e.g., dynein). Both motors operate through MT-MT interactions. The minus-end motor also mediates MT-membrane interactions, as described below. To determine MT-motor interactions, a spatial search is conducted. A grid 24×24 μm in size is placed over the simulation domain and divided into 128×128 bins. A rasterization of each MT segment, based on the defined grid, is computed using Bresenham's line algorithm (12). The resulting integer bin numbers from the rasterization are updated with the MT segment number. Similarly, each motor is placed in an integer bin based on its position. To determine potential motor-MT interactions, only motors and MTs that occupy common bins need to be considered, which effectively eliminates a large portion of the search space. It is important to note that the number of bins must be chosen to ensure that the grid resolution, r_{grid}, is much greater than the capture radius of the motor, r_{motor}.

Motors are assumed to have two heads acting independently for plus-end motors, and are coupled in the case of minus-end motors. Motors can assume one of three states: unbound, single-head bound, and double-head bound. If the motor occupies the same bin as a filament, the distance between each filament and motor is computed. If a filament is within the capture radius, it is bound to the first available unbound head. Unbound motors can bind up to two distinct filaments. Motors that remain unbound diffuse following two-dimensional Brownian motion (10,13) with diffusion coefficient D_{motor}.

Single-head bound motors are probabilistically checked for unbinding, and are checked for additional MT binding of the unbound head. Motors that remain single-head-bound take a step of size $v_{motor}\Delta t$ along the MT in the direction dictated by the motor type, where v_{motor} is the motor velocity and Δt is the computation time step. Like single-head motors, each head in a doubly bound motor is checked stochastically for unbinding. Unbinding of a single head results in the bound head taking the appropriate step. If both heads remain bound, they crosslink the MTs, modeled as a stiff spring of strength k_{con}, and also exert a force that is dependent on motor type. For plus-end motors, the heads act independently. Each head exerts force directed along the MT in the direction opposing the step. The probability of each head taking a step is based on the external load applied to the bound MT. For minus-end motors, the heads are dependent, and the probability of taking a step is based on the external load on each MT. On a doubly bound minus-end motor, only one head can move at each time step.

Minus-end motors found close to the membrane can also have one free head bind to the membrane. When bound to the membrane, the motor acts as a mechanical tether to a bound MT. The motor does not step along the membrane, but can step and exert force on the bound MT as described above. The reaction force is also coupled to the membrane.

Collision detection

To determine collision between motors, MTs, and the membrane, a similar rasterization algorithm is used. A coarse 64×64 grid is placed over the complete domain and the segments that make up the membrane are rasterized and binned. For motor-membrane collisions, the motor positions are binned on the coarse grid, and those occupying the same bin as a membrane segment are considered candidates for collision. The distance between the unbound motors and membrane segments is computed. Those motors within the interaction radius of the membrane are assumed to undergo an elastic collision with the stationary cell membrane.

A similar computation is performed for the MT-membrane interaction. The MTs are rasterized using the coarse grid. Using the previously rasterized membrane, a binary mask is created that shows bins containing both MTs and membrane segments. The distance between the membrane segments and MTs is computed. MTs that fall within the interaction radius of the membrane are potential candidates for collision. The interaction between the MT and the membrane is dependent on the angle of incidence of the MT and the membrane surface. The angle between the filament and the normal on the membrane is computed. MTs that meet the membrane at angles $> 45^{\circ}$ slide along the membrane; otherwise, they push the membrane. When a filament is not sliding, the normal component of the force on the membrane is reduced to zero, with the reaction force being applied outwardly normal on the membrane segment. Stiction forces the parallel component of the force to be zero. For sliding MTs, the normal component of the force on the MT is reduced to zero, and the reaction force is applied to the membrane. The slide condition indicates that stiction no longer occurs and the MT is free to slide along the membrane. The parallel component of the force is reduced by the sliding friction, μF_n, where F_n is the normal component of the force and μ is the coefficient of sliding friction. The reaction force is also applied to the affected membrane segment.

Degree of focus calculation

An MT is said to be focused if its minus end is close enough (25% of the MT length; similar results were obtained using other length thresholds) to one of two spindle focal points. The degree of focus is the ratio between the number of focused, free minus ends and the total number of free MTs. In simulations with asters, these serve as the spindle focal points. Determining the latter in simulations without seeded asters is more complex. The first step is to compute the most probable location for each aster based on the position of the free MTs. The distances between all minus ends are computed; those greater than the length of one MT are not considered close and not used in the aster position calculation. The distance between the minus end of the MT under consideration and all other free MTs is computed for each MT. The MT with the lowest separation distance is chosen as the first focal point. The second is chosen based on the same criteria, but with the condition that it must be at least one MT length away from the first. The focal points can vary from MT to MT during the simulation based on the density of MT minus ends. The spindle length is defined as the distance between the two computed spindle focal lengths.

Synthetic microscope images

The membrane and its components are visualized as synthetic fluorescent images. The positions of MTs (blue), plus-end (red) and minus-end (green) motors, and the membrane (yellow) are separately rasterized on a 256×256 pixel domain (8 pixels per μm). Brighter colors indicate higher density. The channels are added together to form a composite image that is then filtered using a Gaussian filter to simulate microscope optics (14).

RESULTS

An enclosing viscoelastic membrane aids spindle focusing

To test the hypothesis that an enclosing membrane aids the formation of the mitotic spindle, we first carried out simulations on a system of MTs and motors not contained by a membrane. We studied two cases: cells containing only a random orientation of free MTs (Fig. 1 *B*), and cells having both established asters and free MTs (Fig. 1 *C*). In both cases the MTs and motors were initialized around a circle but were free to move thereafter. Simulations of a cell with no astral MTs showed no significant focusing of the MT minus ends, which were directed radially from the center where the plus ends were assembled by the plus-end motors (Fig. 1 *B*). In simulations with astral MTs, the asters separated. Free MTs (those not associated with an aster) showed no appreciable increase in focus from their starting condition (Fig. 1 *C*).

We next considered the effect that an enclosing membrane has on the system for cells without (Fig. 2) and with astral MTs (see Fig. S1 in the Supporting Material). This membrane, first represented by a rigid circular shell, served as an impenetrable barrier to MT movement and motor diffusion as well as a binding site for the minus-end-directed motor. Most MTs in these simulations sorted into opposite sides of the membrane by the action of the motors. However, these MTs did not focus, nor did a spindle morphology arise (Fig. 2 *A* and Fig. S1 *A*). We next modified the membrane model to allow deformation by both elongation and bending (Fig. 2 *A*). These local deformations, combined with the ability of MTs to slide along the membrane, resulted in focusing of the free MTs in a region surrounding the seeded asters. As the membrane deformed, it eventually exerted sufficient force to counterbalance the effect of the MT motors. As the spindle length approached the length of two MTs (10 μm), the degree of overlap

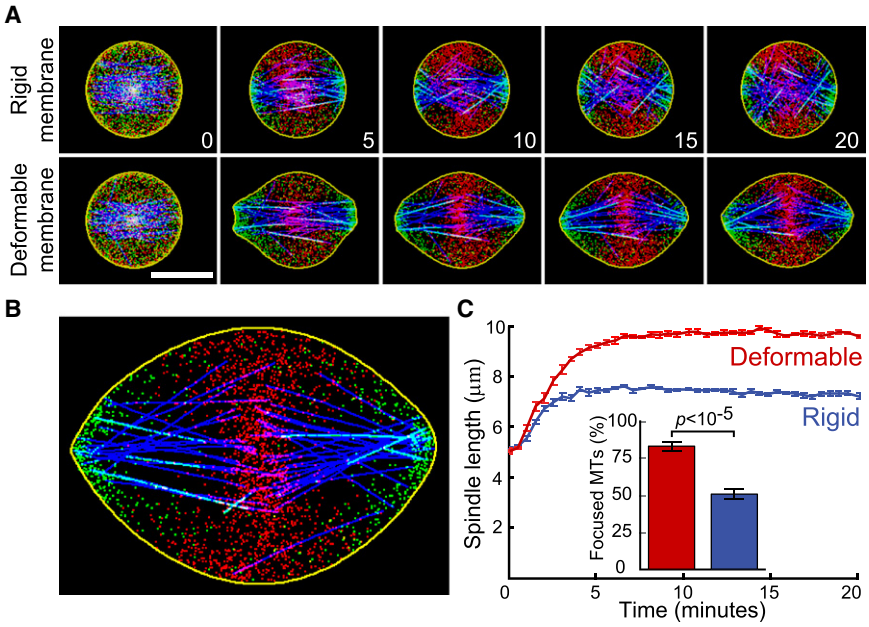

FIGURE 2 Deformable membrane enclosing the mitotic spindle helps to focus MTs. (*A*) Representative simulations for cells that are enclosed by a rigid or deformable membrane. In both cases the plus-end motors push away MTs toward the membrane. If this membrane is deformable, it provides a counter force that eventually reaches a balance. (*B*) Enlarged image of a spindle at steady state. (*C*) The elastic nature of the membrane helps to resist the force exerted by the MT plus ends pushing on the MTs and eventually reaching a steady-state length. The inset shows the percentage of focused MTs 20 min after the start of the simulation ($n = 12$, Student's *t*-test). The error bars denote the standard error. The scale bar represents 5 μm.

between MTs was small, which limited the additional force that the motors could exert. This allowed the spindle length to reach a steady state (Fig. 2, *B* and *C*). The elastic membrane also included a small viscous component; without it, oscillations in the membrane could be observed (not shown).

We quantified the degree of focusing in the resultant spindles. The MTs in cells without asters focused much better than those in cells with only a rigid membrane (80% vs. 50%, $p < 10^{-5}$, Student's *t*-test; Fig. 2 *C*). Simulations of cells with asters revealed similar behavior, but the length of the spindle was shorter and the degree of focusing was smaller (Fig. S1). Overall, however, the presence of the deformable membrane made a significant difference in comparison with a rigid membrane.

Varying membrane elasticity controls spindle length

We next sought to establish how the physical properties of the membrane influence the ability of MTs to assemble into an organized spindle. To test how the elasticity of the membrane regulates the ability of the spindle to achieve focus, we simulated the system using different elastic moduli for the membrane and compared the morphology of the mitotic spindle as well the rate at which the system reached a steady state. Cells with and without asters organized a spindle for all the elastic moduli tested (Fig. 3 *A* and Fig. S2 *A*). In cells without asters, smaller elastic moduli led to longer spindles—particularly early in the process—because the elastic force provided by the membrane was smaller. These cells also reached steady state faster. However, the degree of focusing was smaller than that of cells with more elastic membranes (Fig. 3 *B*). We saw similar, though smaller, effects in cells with astral MTs, i.e., higher elasticity led to shorter but more-focused spindles (Fig. S2).

In the above-described simulations, the enclosing mitotic membrane was spatially homogeneous. We also simulated system using a spatially heterogeneous membrane with two randomly placed regions of reduced elasticity, each with 10% of the initial membrane perimeter and only 10% of the default elasticity. These simulations gave rise to poorly focused spindles with severe morphological defects, as the minus ends became stuck in these pockets (Fig. 3 *C*).

The concentration and ratio of motor proteins regulate the ability to focus MTs

Plus- and minus-end-directed motors provide the forces that help to sort the MTs into the two ends of the cell, and are then counterbalanced by the elastic forces from the membrane. We investigated the role played by these motors in spindle formation (Fig. 4). Decreasing the number of plus-end motors resulted in slower separation of the spindles. This effect was transient, however, as the steady state reached was approximately the same for all the simulations. Increasing the number of motors beyond the default value had a relatively weak effect on cells without asters (Fig. 4, *A* and *B*) but induced significant differences for cells with asters (Fig. S3, *A* and *B*). Not surprisingly, changing the number of minus-end motors had the opposite outcome: reducing the number of minus-end motors in cells without asters resulted in faster spindle formation, whereas increasing the number made the cell reach steady state more slowly (Fig. 4, *C* and *D*). Altering the number of

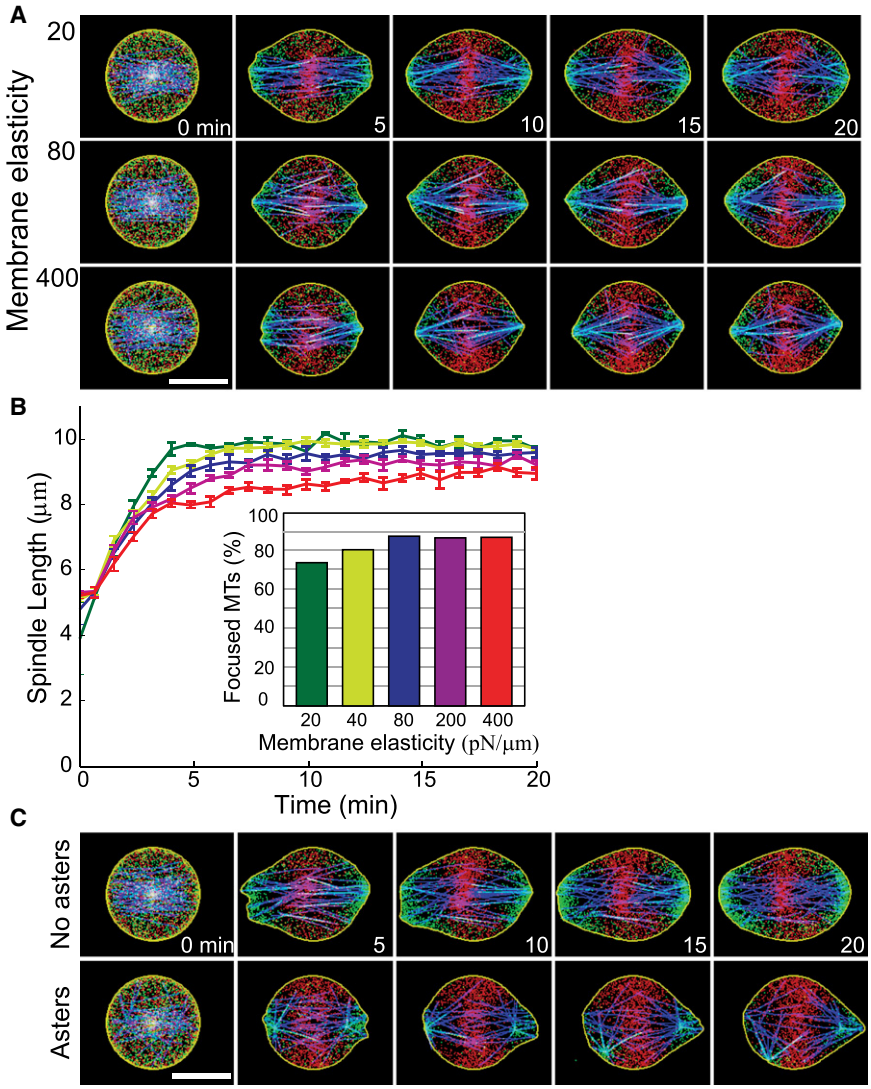

FIGURE 3 Steady-state length and shape of the mitotic spindle depends on the membrane elasticity. (*A*) Sample simulations for cells in which the membrane's elasticity has been changed from 20 to 400 pN/μm. (*B*) Spindle length as a function of time. The inset shows the percentage of focused MTs 20 min after the start of the simulation. (*C*) Sample simulations in which the membrane has two pockets of low elasticity demonstrate that spatial heterogeneities in the membrane elasticity give rise to mitotic spindle defects. Scale bars represent 5 μm.

minus-end motors in cells with asters had a reduced effect (Fig. S3, *C* and *D*).

Recent studies have shown that some MT crosslinkers, including nonmotor MAPs of the Ase1p family, affect spindle formation (15,16). These proteins bind preferentially to antiparallel overlapping MTs in a relatively immobile state and may act as a scaffold in the spindle midzone (17). To investigate their role in our simulations, we created a crosslinker with two heads that had no processive activity. Spindles in these simulations still focused, but reached steady state more slowly (Fig. 4 *E*), consistent with the idea that crosslinkers provide added resistance to the force separating antiparallel linked MTs.

The length of the mitotic spindle is determined by the MT length and the balance of forces

Changing the elastic properties of the membrane (Fig. 3) and the relative number of motors (Fig. 4) primarily changed the time required for the spindle to reach its steady state but did not affect the final spindle length, which was only slightly less than twice the MT length. We hypothesized that, at steady state, the forces that motors generate by sliding antiparallel MTs against the membrane are balanced by the force generated by deformation of the elastic membrane. We further tested this hypothesis through an analytic model that quantifies these forces (Supporting Material). This model considers only the net effect of motors pushing MTs and assumes that the MTs are already focused on a single spot. It also explores the effect of varying MT length. Results from this model suggest that the spindle length is approximately proportional to the MT length and the net number of motors, as the force generated by the motors depends on the region of MT overlap, and inversely proportional to the membrane elasticity (Fig. 5 *A*).

To test this model, we carried out simulations in which we varied the expected MT length. These simulations showed a similar dependence of steady-state spindle length on MT

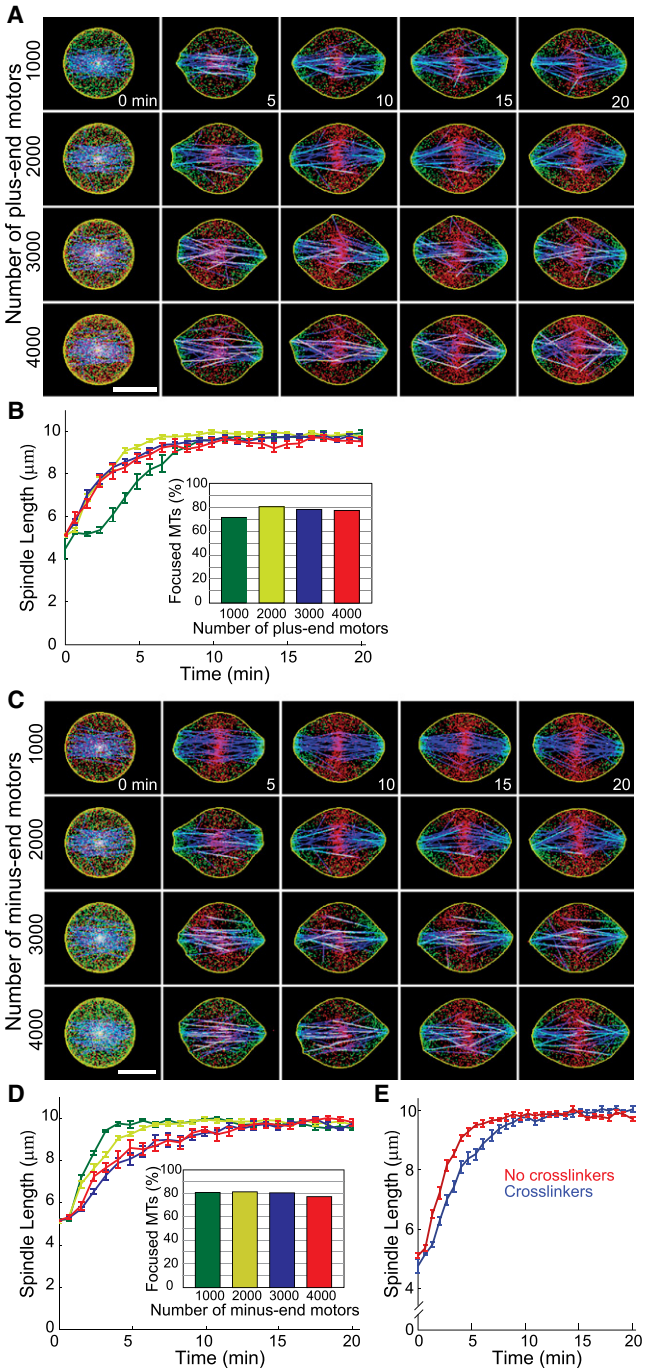

FIGURE 4 Varying the number MT motors leads to changes in focusing and the speed at which the system reaches steady state. (*A* and *B*) Sample simulation results in which the number of plus- or minus-end motors varies from 1000 to 4000. The other motor number is kept constant at 2000. (*C* and *D*) Degree of minus-end focusing as a function of time. The inset shows the percentage of focused MTs 20 min after the start of the simulation. (*E*) The presence of passive crosslinkers slows the progression toward steady state, but not the spindle length. The scale bars represent 5 μm. The error bars correspond to the standard error.

length and, to a smaller degree, on membrane elasticity (Fig. 5, *B* and *C*). We also tested the effect that increasing the length of only a few MTs has on spindle length. For

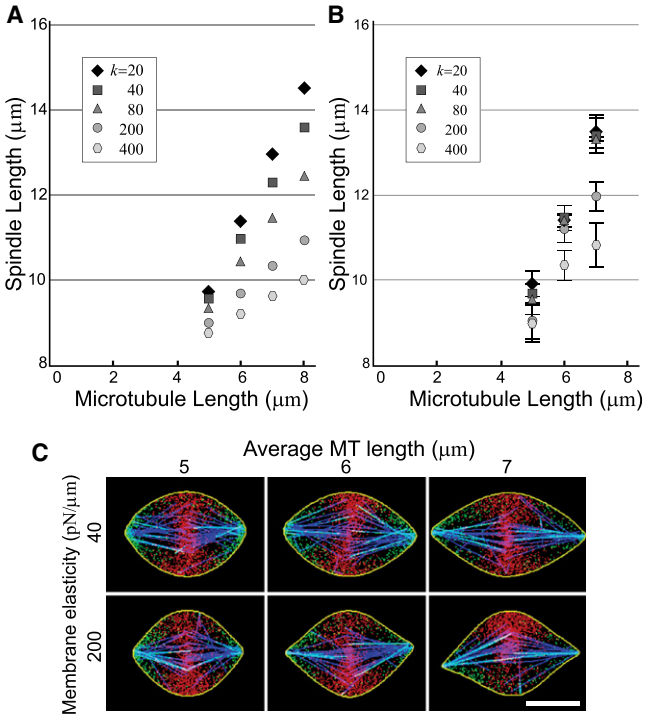

FIGURE 5 Spindle length depends on the MT length and the balance of forces acting on them. (*A*) Based on an analytic model of the balance of forces at steady state, the spindle length increases with the MT length and inversely with MT length and inversely with membrane elastic modulus (k, in pN/μm). (*B*). Steady-state spindle lengths obtained from the simulations show similar dependences. Error bars are the standard deviation. (*C*) Sample steady-state images of these simulations. The scale bar represents 5 μm.

example, lengthening 10 MTs to 7.5 μm (leaving the others to have an expected length of 5 μm) increased the spindle length. In these simulations, the longer MTs tended to create the initial indentations that drew in the other (shorter) MTs (not shown).

DISCUSSION

The formation of the mitotic spindle represents one of the prime examples of complex biological integration, whereby large numbers of interacting proteins come together and give rise to a new structure. Not surprisingly, computational models can be extremely useful not only for testing hypotheses about the nature of the interactions, but also for developing new hypotheses (5,14,18). Here we developed a computational model based on biophysical interactions among MTs, MT motors, and a mitotic membrane to ascertain possible roles for this membrane.

We determined that the presence of a membrane helps to restrict the motion of both MTs and molecular motors subject to Brownian motion, and to keep these in the region where the spindle is to be formed. Whereas the binding of motors to the MTs slows down the effective diffusion of the motors, we still found that in the absence of an enclosing

membrane, MT motors diffused away, reducing their ability to effect spindle formation. Thus, the membrane allows for increased concentration of MT motors. Although we did not include other mitotic assisting proteins in our model, a similar effect facilitating spindle formation would apply to these species as well.

Our simulations also indicate that the presence of a deformable membrane aids in establishing distinct focal points for MT minus ends. How does this focusing take place? As parallel aligned MTs are pushed away from each other by double-headed plus-end motors, the MTs push against the membrane, causing local deformations (Fig. 6, *A* and *B*). The net force exerted on the membrane in regions between MTs induces a geometry that causes the MTs to slide along the membrane, leading to focusing (Fig. 6, *C–E*). Membrane-aided focusing of MTs is reminiscent of a model in which the lipid bilayer drives and stabilizes the emergence of filopodium-like actin protrusions (19,20). A recently published mathematical model of motor-MT bundles considered two possible means of anchoring the minus end of MTs to the pole—clamping and hinging—and determined that hinging led to more realistic spindle shapes (21). At steady state, the focus generated by the mitotic membrane provides such a hinge.

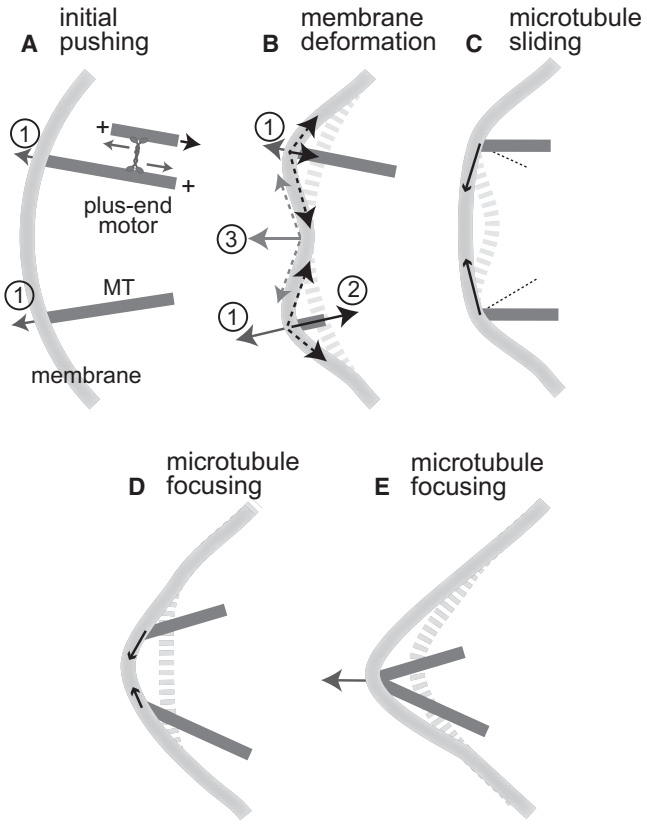

FIGURE 6 Model for mitotic membrane-enabled spindle focusing. (*A*) Antiparallel oriented MTs are pushed away from each other and onto the mitotic membrane by plus-end motors exerting force on the membrane (*circle 1*). (*B*) The force deforms the membrane, which provides an elastic force to resist (*circle 2*). This force can be resolved into normal and tangent components (*dotted lines*). The tangential component is resisted by a force (*circle 3*) that acts to restore the spherical shape. (*C*) The resultant deformation leads to a changed geometry in which MTs push at an angle that is not normal to the membrane. If this angle is large enough, the MTs will slide, rather than push the membrane. (*D*) The sliding of the MTs helps to focus the minus ends. (*E*) When focused, the MTs combine their pushing force.

Initial spindle assembly and elongation require a proper balance of forces (22–26). In our model, the net action of the MT motors provides the force that pushes the MT on the membrane. The deformation of this membrane places the MTs under compression, thereby resisting the MT motors. Because the total MT motor force is limited by both the number of available MT motors and the length of the MT antiparallel overlap, the length of the assembled spindle is regulated by the elasticity of the membrane. Our simulations showed that increasing the membrane elasticity (Fig. 3 and Fig. S2) or decreasing the net motor force (Fig. 5 and Fig. S3) led to shorter spindles. Recent studies in *Drosophila* early embryos support the finding that the nature of the mitotic spindle arises from the balance of forces provided by the MT motors and the elastic membrane (27). It is perhaps counterintuitive to find that less-elastic membranes give rise to slower focusing. However, a reduction in membrane elasticity means that less force is required to deform the membrane, and this allows single MTs to induce local deformations in the membrane. These local deformations temporarily capture MTs, slowing the ability of the spindle to focus. Such membrane deformations are reduced on elastically stiff membranes, decreasing local pockets of MTs and resulting in faster spindle focusing. We found that simulations in which the membrane had spatially heterogeneous elastic properties gave rise to even slower spindle focusing, as MTs were captured by these isolated pockets of low elasticity (Fig. 4).

All of our simulations were carried out for systems with or without asters. The presence of astral MTs actually hindered MT focusing on the membrane. This is because, as the asters were pushed against the membrane, some of the astral MTs were also pushed against the membrane, which prevented their minus ends from reorienting and thus precluded them from focusing.

Invariably, simulations like those carried out here involve a compromise between fidelity and complexity. For example, the MTs in our simulations are of varying but fixed length. Previous simulations with and without dynamic instabilities showed similar MT organization (28). It has been shown that MTs pushing against a rigid barrier increase the rate of catastrophe by limiting the rate of growth (29).

We avoided three-dimensional simulations because of the computational burden involved in combining deformable membranes in three dimensions with the collision-detection algorithms used. However, the results should still apply. There are several processes that together lead to the

focusing and stabilization reported here. First, when MTs push a deformable membrane, they alter the geometry, causing a local indentation on the membrane. When this deformation is large, other MTs slide into its basin of attraction, allowing them to add to the outward force (Fig. 6). This process ends when the net force of the motors is balanced by the elastic force of the membrane. As the spindle elongates, the overlap between antiparallel aligned MTs decreases, which in turn decreases the number of motors that can bind and push apart the MTs. Thus, there are two forms of negative feedback: one due Hooke's law, and one due to the decreasing length of overlap. All of these processes will remain valid in three dimensions. In three dimensions, MTs push and deform an elastic two-dimensional membrane, causing a concave indentation that acts as a funnel drawing in other MTs. When the incidence angle is sufficiently large, these MTs will still slide toward the center of the funnel. Eventually, the forces will be balanced as the pushing force decreases (because of the smaller overlap in antiparallel aligned MTs) and the restoring force of the elastic membrane increases. We do foresee, however, that the process may be slower in three dimensions because the extra degree of freedom involved may delay MTs joining as bundles.

There are two main systems that could mimic the function of the membranes modeled here that could be responsible for spindle assembly. Lamin B, an intermediate filament protein that is associated with the mitotic spindle, provides elastic resistance reminiscent of a molecular shock absorber (11) and has been shown to be required for spindle assembly (2). These filaments are assembled into an interconnected structure and regulated by the motor protein dynein, and the linking protein Nudel (30). Dynein and nudel were both found to be colocalized with the assembled LB3 matrix.

In addition to the lamin matrix, a second membrane has been shown to surround the mitotic spindle. This membrane is thought to form from sections of the broken-down nuclear envelope and endoplasmic reticulum membrane (4). A target protein, epsin1, has been localized to these membrane sections and been shown to be responsible for membrane deformation (31). It is thought that espin1 does not act directly on the MTs, but rather acts indirectly by altering the mitotic membrane organization. A knockdown of epsin results in spindle defects, indicating that epsin is required to induce membrane curvature and shape the spindle assembly. The extendibility of the membrane is driven by the interaction between lamin and its linking proteins, whereas the ability of the membrane to bend is largely governed by the protein epsin. This leads to two distinct yet connected modes to consider in the ability of a spindle to self-assemble in the presence of a membrane. The spindle defects we found in our simulations using heterogeneous membranes are representative of the defects seen in epsin knockdown membranes (31).

SUPPORTING MATERIAL

Analytical model derivation and four figures are available at http://www.biophysj.org/biophysj/supplemental/S0006-3495(10)01203-8.

This work was supported in part by the National Institutes of Health (GM056312 to Y.X. and GM086704 to P.A.I.) and the National Science Foundation (0621740 to P.A.I.). Y.Z. is an investigator of the Howard Hughes Medical Institute.

REFERENCES

1. Johansen, K. M., and J. Johansen. 2002. Recent glimpses of the elusive spindle matrix. *Cell Cycle.* 1:312–314.
2. Tsai, M. Y., S. Wang, …, Y. Zheng. 2006. A mitotic lamin B matrix induced by RanGTP required for spindle assembly. *Science.* 311: 1887–1893.
3. Zheng, Y. 2010. A membranous spindle matrix orchestrates cell division. *Nat. Rev. Mol. Cell Biol.* 11:529–535.
4. Zheng, Y., and M. Y. Tsai. 2006. The mitotic spindle matrix: a fibromembranous lamin connection. *Cell Cycle.* 5:2345–2347.
5. Mogilner, A., R. Wollman, …, J. Scholey. 2006. Modeling mitosis. *Trends Cell Biol.* 16:88–96.
6. Mogilner, A., and E. Craig. 2010. Towards a quantitative understanding of mitotic spindle assembly and mechanics. *J. Cell Sci.* 123:3435–3445.
7. Nédélec, F. 2002. Computer simulations reveal motor properties generating stable antiparallel microtubule interactions. *J. Cell Biol.* 158:1005–1015.
8. Channels, W. E., F. J. Nédélec, …, P. A. Iglesias. 2008. Spatial regulation improves antiparallel microtubule overlap during mitotic spindle assembly. *Biophys. J.* 94:2598–2609.
9. Civelekoglu-Scholey, G., L. Tao, …, J. M. Scholey. 2010. Prometaphase spindle maintenance by an antagonistic motor-dependent force balance made robust by a disassembling lamin-B envelope. *J. Cell Biol.* 188:49–68.
10. Nedelec, F. J., and D. Foethke. 2007. Collective Langevin dynamics of flexible cytoskeletal fibers. *N. J. Phys.* 9:427.
11. Dahl, K. N., S. M. Kahn, …, D. E. Discher. 2004. The nuclear envelope lamina network has elasticity and a compressibility limit suggestive of a molecular shock absorber. *J. Cell Sci.* 117:4779–4786.
12. Bresenham, J. E. 1965. Algorithm for computer control of a digital plotter. *IBM Syst. J.* 4:25–30.
13. Howard, J. 2001. Mechanics of Motor Proteins and the Cytoskeleton. Sinauer Associates, Sunderland, MA.
14. Gardner, M. K., and D. J. Odde. 2010. Stochastic simulation and graphic visualization of mitotic processes. *Methods.* 51:251–256.
15. Janson, M. E., R. Loughlin, …, P. T. Tran. 2007. Crosslinkers and motors organize dynamic microtubules to form stable bipolar arrays in fission yeast. *Cell.* 128:357–368.
16. Kapitein, L. C., B. H. Kwok, …, E. J. Peterman. 2008. Microtubule cross-linking triggers the directional motility of kinesin-5. *J. Cell Biol.* 182:421–428.
17. Peterman, E. J., and J. M. Scholey. 2009. Mitotic microtubule crosslinkers: insights from mechanistic studies. *Curr. Biol.* 19:R1089–R1094.
18. Schaffner, S. C., and J. V. José. 2006. Biophysical model of self-organized spindle formation patterns without centrosomes and kinetochores. *Proc. Natl. Acad. Sci. USA.* 103:11166–11171.
19. Liu, A. P., D. L. Richmond, …, D. A. Fletcher. 2008. Membrane-induced bundling of actin filaments. *Nat. Phys.* 4:789–793.
20. Atilgan, E., D. Wirtz, and S. X. Sun. 2006. Mechanics and dynamics of actin-driven thin membrane protrusions. *Biophys. J.* 90:65–76.
21. Rubinstein, B., K. Larripa, …, A. Mogilner. 2009. The elasticity of motor-microtubule bundles and shape of the mitotic spindle. *Phys. Biol.* 6:016005.

22. Mountain, V., C. Simerly, …, D. A. Compton. 1999. The kinesin-related protein, HSET, opposes the activity of Eg5 and cross-links microtubules in the mammalian mitotic spindle. *J. Cell Biol.* 147:351–366.

23. Dumont, S., and T. J. Mitchison. 2009. Force and length in the mitotic spindle. *Curr. Biol.* 19:R749–R761.

24. Sharp, D. J., H. M. Brown, …, J. M. Scholey. 2000. Functional coordination of three mitotic motors in *Drosophila* embryos. *Mol. Biol. Cell.* 11:241–253.

25. Tanenbaum, M. E., L. Macůrek, …, R. H. Medema. 2008. Dynein, Lis1 and CLIP-170 counteract Eg5-dependent centrosome separation during bipolar spindle assembly. *EMBO J.* 27:3235–3245.

26. Ferenz, N. P., R. Paul, …, P. Wadsworth. 2009. Dynein antagonizes Eg5 by crosslinking and sliding antiparallel microtubules. *Curr. Biol.* 19:1833–1838.

27. Civelekoglu-Scholey, G., and J. M. Scholey. 2010. Mitotic force generators and chromosome segregation. *Cell. Mol. Life Sci.* 67:2231–2250.

28. Pinot, M., F. Chesnel, …, Z. Gueroui. 2009. Effects of confinement on the self-organization of microtubules and motors. *Curr. Biol.* 19:954–960.

29. Janson, M. E., M. E. de Dood, and M. Dogterom. 2003. Dynamic instability of microtubules is regulated by force. *J. Cell Biol.* 161: 1029–1034.

30. Ma, L., M. Y. Tsai, …, Y. Zheng. 2009. Requirement for Nudel and dynein for assembly of the lamin B spindle matrix. *Nat. Cell Biol.* 11:247–256.

31. Liu, Z., and Y. Zheng. 2009. A requirement for epsin in mitotic membrane and spindle organization. *J. Cell Biol.* 186:473–480.

32. Chakravarty, A., L. Howard, and D. A. Compton. 2004. A mechanistic model for the organization of microtubule asters by motor and non-motor proteins in a mammalian mitotic extract. *Mol. Biol. Cell.* 15:2116–2132.

33. Toba, S., T. M. Watanabe, …, H. Higuchi. 2006. Overlapping hand-over-hand mechanism of single molecular motility of cytoplasmic dynein. *Proc. Natl. Acad. Sci. USA.* 103:5741–5745.

34. King, S. J., and T. A. Schroer. 2000. Dynactin increases the processivity of the cytoplasmic dynein motor. *Nat. Cell Biol.* 2:20–24.